optica

Active hyperbolic metamaterials: enhanced spontaneous emission and light extraction

T. GALFSKY,[1,2] H. N. S. KRISHNAMOORTHY,[1,2] W. NEWMAN,[3] E. E. NARIMANOV,[4] Z. JACOB,[3] AND V. M. MENON[1,2,*]

[1]Department of Physics, City College, City University of New York (CUNY), New York, New York 10031, USA

[2]Department of Physics, Graduate Center, City University of New York (CUNY), New York, New York 10016, USA

[3]Department of Electrical and Computer Engineering, University of Alberta, Edmonton, Alberta T6G 2V4, Canada

[4]Birck Nanotechnology Center, School of Computer and Electrical Engineering, Purdue University, West Lafayette, Indiana 47907, USA

*Corresponding author: vmenon@ccny.cuny.edu

Received 6 October 2014; revised 18 November 2014; accepted 24 November 2014 (Doc. ID 224486); published 16 January 2015

Hyperbolic metamaterials (HMMs) have recently garnered much attention because they possess the potential for broadband manipulation of the photonic density of states and subwavelength light confinement. These exceptional properties arise due to the excitation of electromagnetic states with high momentum (high-*k* modes). However, a major hindrance to practical applications of HMMs is the difficulty in coupling light out of these modes because they become evanescent at the surface of the metamaterial. Here we report the first demonstration, to our knowledge, of simultaneous spontaneous emission enhancement and outcoupling of high-*k* modes in an active HMM using a high-index-contrast bullseye grating. Quantum dots embedded inside the metamaterial are used for local excitation of high-*k* modes. This demonstration could pave the way for the development of photonic devices such as single-photon sources, ultrafast LEDs, and true nanoscale lasers.

OCIS codes: (160.3918) Metamaterials; (250.5403) Plasmonics; (230.5590) Quantum-well, -wire and -dot devices.

http://dx.doi.org/10.1364/OPTICA.2.000062

Control of spontaneous emission (SE) is of both fundamental and technological importance. Conventional approaches to enhance SE by modifying the dielectric environment relies on resonant phenomena such as cavity resonance where the SE rate is enhanced over a narrow spectral range. Introducing an outcoupling mechanism then reduces the quality factor of the cavity and thereby the enhancement in SE rate. For applications requiring narrow wavelength response, photonic crystal cavities have been used to enhance emission by optimizing the structural parameters for directional emission and maximizing the Q factor for a given cavity mode [1,2]. An alternate approach that has recently attracted much attention is the use of hyperbolic metamaterials (HMMs) where the Purcell enhancement stems from high-momentum states called high-k modes, which exist in a broad spectral range and are a nonresonant phenomenon [3,4].

HMMs are artificially engineered substructured materials so named for possessing hyperbolic dispersion. HMMs in optical frequencies can be realized by metal–dielectric stacks supporting coupled surface plasmon polaritons (SPPs). Quantum emitters placed inside or on top of these structures have been shown to experience radiative decay rate enhancement, with the former having greater effect due to better coupling to high-k modes [5–9]. Patterning of HMMs has been shown to strongly enhance radiative decay rate for quantum emitters [8,10]; however, to the best of our knowledge, simultaneous enhancement of radiative decay and light extraction had not been shown to date. Following the proposal of a bullseye grating as an outcoupling mechanism [11], we show in this Letter, for the first time to our knowledge, experimental verification of simultaneous enhancement of SE and outcoupling of high-k modes generated by embedded dipole emitters, using a high contrast bullseye grating.

The structure [shown schematically in Fig. 1(a)] consists of seven periods (7P) of alternating layers of aluminum oxide (Al_2O_3) at ~20 nm thickness and silver (Ag) at ~12 nm, with ultrathin Germanium (Ge) (~1–2 nm thick) seed in between. A spin-coated active layer of quantum dots (QDs) is embedded in the middle of the fifth Al_2O_3 layer (for full details of the fabrication see Sections 1 and 5 of Supplement 1). In the fabricated structure, a single period is defined as a unit cell of Al_2O_3/Ge/Ag layers. The fabrication is conducted in two stages. Stage 1 consists of four periods (4P) and an additional Al_2O_3 layer with embedded QDs. Stage 2 completes the full seven period (7P) structure. We determined the exact thickness of the dielectric and metallic layers from cross-sectional imaging with a transmission electron microscope (TEM) [Fig. 1(b)], and the permittivity constants of the thin layers of Ag/Ge and Al_2O_3 were determined from spectroscopic ellipsometry measurements. Knowing the layers' permittivity and the exact fill fraction of metal in the structure, we calculated the components of the effective anisotropic permittivity using effective medium theory [Fig. 1(c) and Section 2 of Supplement 1). Above a wavelength of ~440 nm, the permittivity components parallel (‖) and perpendicular (⊥) to the interface have opposite signs, which lends a hyperboloid shape to the isofrequency contour (IFC) according to the dispersion relation equation

$$\frac{k_x^2 + k_y^2}{\varepsilon_\perp} + \frac{k_z^2}{\varepsilon_\parallel} = \frac{\omega^2}{c^2}. \quad \textbf{(1)}$$

The hyperbolic shape of the IFC is schematically shown in the overlay of Fig. 1(c) along with the spherical IFC of air, depicting the issue of mode mismatch between free space and HMM. The spectrum of the QDs used in the experiment is also shown in Fig. 1(c) as a dashed line.

In a HMM, the origin of the high-k modes stems from the coupling between SPPs supported by individual metal–dielectric interfaces. The exact dispersion of the modes depends on the multilayer period (lattice pitch) and metal–dielectric layer thicknesses where the highest allowed propagating k vector is limited by the finite period of the multilayer. These coupled plasmonic modes create local enhancement in the photonic density of states (PDOS) and provide a radiative decay channel for quantum emitters [5,11].

To test the effect of high-k modes on spontaneous decay rate, a fluorescence lifetime imaging microscopy setup (see Section 5 of Supplement 1) was employed to obtain the lifetime distribution in an area size of 20 μm × 20 μm of four samples. Figure 1(d) shows the lifetime distribution of 7P and 4P in comparison to a control sample consisting of a single period (1P), and a reference sample of QDs on a glass substrate. We observe that the measured lifetime becomes shorter as the number of periods is increased, indicating the presence of high-k modes. The measured reduction is comparable to previous reports [6,7], with the 7P structure showing decay rate enhancement $\beta \equiv t_{\mathrm{Ref}}/t_{\mathrm{7P}} = 9.5$ relative to glass, where t_{Ref} and t_{7P} are the average lifetimes of the QDs on glass and in the 7P structure, respectively. These values are extracted by fitting the distribution with an asymmetric peak function. In addition to the measurement, the expected decay rate enhancement was analytically calculated, and shows a good match to the experimentally obtained values (see Section 3 of Supplement 1).

It is appropriate to note that, in plasmonic materials, a part of the lifetime shortening could be attributed to nonradiative metal quenching. The quenching effect for this type of HMM has been rigorously investigated in previous work [11], and the location of the emitters has been selected to minimize the effect of quenching.

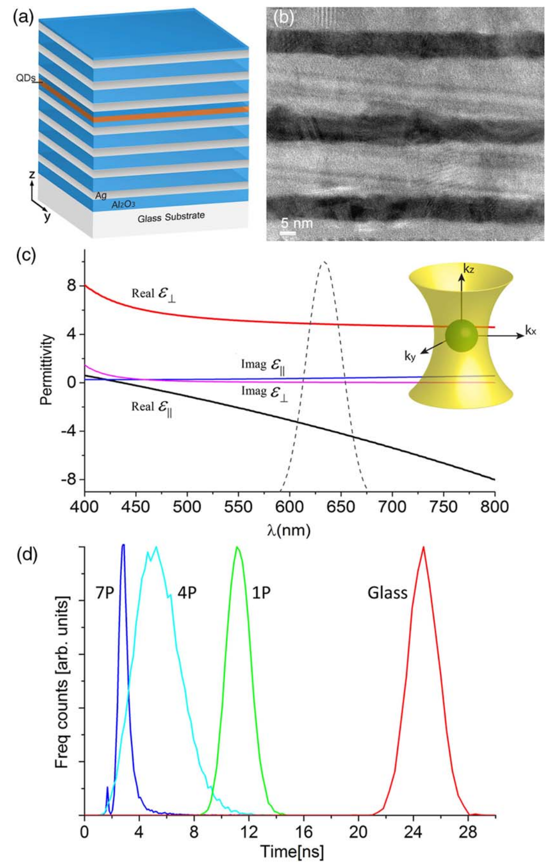

Fig. 1. (a) Schematic of the HMM composed of Ag/Al_2O_3. (b) Cross-sectional TEM image showing smooth continuous films of Ag (dark) and Al_2O_3 (bright). (c) Permittivity of the structure as calculated from Effective Medium Theory based on experimentally determined dielectric constants and metal fill fraction. Dotted line corresponds to the emission spectrum of the QDs. Inset, hyperbolic IFC of an ideal HMM overlaid on the spherical IFC of air. (d) Lifetime distribution of QDs on glass, 1P, 4P, and inside a 7P nonpatterned HMM.

To simulate the electric field inside the fabricated structure we used commercial finite-element-method (FEM) software COMSOL. Figure 2(a) maps the electric field generated by a dipole inside the 7P HMM, showing an X-shape radiation pattern known as resonance cone [11,12]. Hyperbolic dispersion also changes the direction of the Poynting vector, which is orthogonally oriented to the IFC and is thus contained within the resonance cone. Therefore, the energy flow due to high-k modes is inherently directed toward the surface of the HMM [11]. However, the electric field becomes evanescent at the air interface so that most of the dipole emission is internally reflected at the top and bottom interfaces, as can be seen in Fig. 2(a). To translate the evanescent field into propagating waves, an appropriate grating structure must be designed.

Due to the difficulty in extending the Green's function approach to arbitrary geometries and random dipole orientations, a numerical approach was used for the grating design. Multiparameter FEM simulations for grating height and periodicity for several fabrication-compatible materials were optimized to

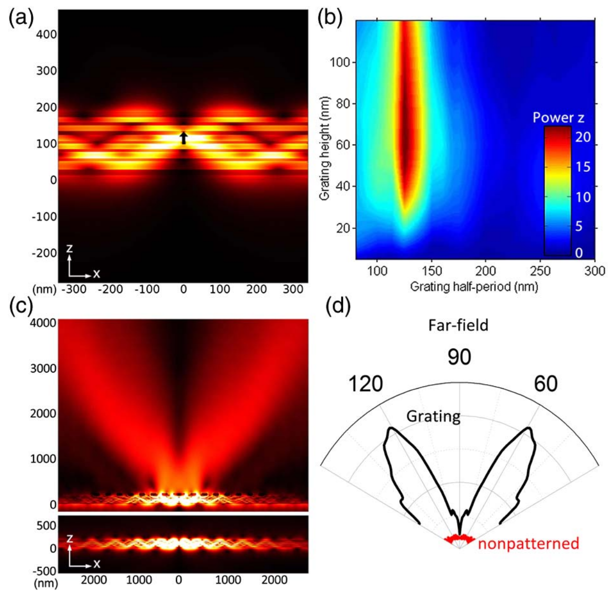

Fig. 2. (a) Simulation of the electric field generated by a vertical dipole placed inside the 7P HMM. Black arrow represents the dipole. (b) Outcoupled power in an angle range of −45° to 45° as a function of grating period and height. (c) Top, outcoupling of the evanescent field by an optimized Ge grating with half period 125 nm and height of 60 nm. Bottom, nonpatterned HMM shown on the same scale. (d) Far-field emission of dipole ensemble (arb. units) for optimized grating and nonpatterned HMM.

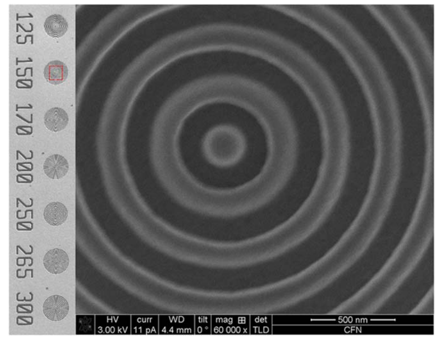

Fig. 3. SEM image of $\Delta = 150$ nm bullseye grating. Left array of gratings with different periods.

maximize outcoupling [Fig. 2(b)]. Despite being lossy in the visible range, Ge was selected for the grating implementation over other compatible dielectrics due to its high index of refraction, which allows it to function as a high-contrast grating (HCG) with air [13], thus aiding the outcoupling of high-k modes (see Section 4 of Supplement 1). The spectral bandwidth of the optimized grating is ~50 nm, which fully covers the emission spectrum of the QDs (see Section 4 of Supplement 1).

In the top panel of Fig. 2(c), we show the near field emission pattern from a 7P HMM with an optimally designed bullseye grating ($\Delta = 125$ nm, $h = 60$ nm). For comparison, the bottom panel shows the emission pattern without a grating outcoupler. In Fig. 2(d), the far-field emission pattern is plotted for a dipole ensemble in an HMM with and without the grating. The ensemble approach is used for calculations and simulations throughout this Letter to account for the random dipole orientations of the QDs and their PL spectrum (see Section 3 of Supplement 1).

To experimentally demonstrate the effect of grating period on outcoupling efficiency, bullseye gratings with half-periods $\Delta = 125$, 150, 170, 200, 250, 265, and 300 nm were patterned onto a polymethyl methacrylate (PMMA) resist layer that was spin-coated on top of the HMM. The gratings written on the PMMA were used as a mask for depositing Ge and realizing the high-contrast bullseye gratings (see Section 5 of Supplement 1). Scanning electron microscope (SEM) images of the $\Delta = 150$ nm grating and an array of gratings with different periodicities are shown in Fig. 3.

The photoluminescence (PL) and lifetime of the patterned HMM were measured simultaneously using the confocal microscope setup described in Section 5 of Supplement 1. Figure 4(a) shows a PL image of the grating array. Enhanced light emission is clearly seen in the gratings while the dark background elucidates the evanescent nature of the high-k modes, which cannot propagate to the far field without an outcoupling mechanism. The bright spots in the emission seen inside the gratings are due to the presence of clusters of QDs formed during spin-coating, and were not included in the image analysis.

The ratio of the average PL intensity from the gratings to the nonpatterned areas is presented in Fig. 4(b), together with the results of numerical calculation of this ratio from FEM simulations. In both simulation and experiment, the amount of outcoupled light increases for smaller grating periods, with $\Delta = 125$ nm yielding an intensity contrast of 20:1 in comparison to the nonpatterned regions. This sharp contrast could only be attributed to outcoupling of multiple high-k modes since no other power flow mechanism exists in the structure. In comparison to the HMM, the 1P control sample shows far smaller contrast between the background and the gratings due to the lack of high-k modes. An additional feature observed in the emission pattern from the HCG is the presence of the dark center. Our simulation of the electric field in the near and far field also show the same dark spot, which is most clearly observed for $\Delta = 125$ nm (see Section 6 of Supplement 1).

In addition to PL intensity, we studied the time dynamics of PL emission of QDs located inside and outside the grating regions. Conventional wisdom dictates that the bullseye gratings will degrade the Purcell enhancement of the QDs, resulting in longer lifetimes as is the case in resonant cavity approaches [1,2]. Counterintuitively, we observe a reduction in lifetime for QDs located under the bullseye (≈1.9 ns) relative to those located away from the bullseye (≈2.6 ns). The inset in Fig. 4(b) shows a fluorescence lifetime map for $\Delta = 125$ nm, where the two regions are clearly observed (lifetime kinetics curves are shown in Section 7 of Supplement 1). We elucidate the physics of this observation below.

Simulations indicate that the Purcell enhancement is nearly equal for a dipole ensemble located below or away from the bullseye. The reason for the relative insensitivity to the outcoupling mechanism is that, in an HMM, the Purcell enhancement for embedded emitters is largely driven by the

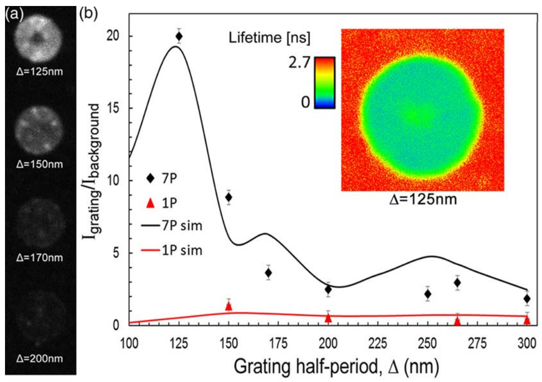

Fig. 4. (a) Confocal microscope image of PL emission from bullseye gratings with half periods $\Delta = 125$, 150, 170, and 200 nm on 7P HMM. The measurements were carried out over a scan area of 10 μm × 40 μm. Details of the measurement technique can be found in Section 5 of Supplement 1. (b) Experimentally measured ratio between the intensity at the center of the grating to that of nonpatterned background for 7P and 1P for different grating periods. Solid lines are the calculated ratios from simulations. Inset, fluorescence lifetime map of $\Delta = 125$ nm.

massive local electric field enhancement that the high-k modes provide at the location of the dipoles. The dielectric grating does scatter these bulk modes into free space; however, it only provides a relatively weak perturbation of the field enhancement and the local PDOS remains largely unperturbed. However, a reduction in lifetime was observed experimentally in the grating region as mentioned above. To understand this observation, one needs to take into account the proportion of outcoupled light emanating from the two-dipole orientations. At locations far from the grating, we only collect the small portion of light emitted by the randomly oriented dipoles, which is uncoupled to high-k modes and can reach the far field without an outcoupling mechanism. In contrast, at the location of the grating, we predominately collect scattered high-k emissions from vertically oriented dipole moments [see Fig. 2(d) and Fig. S4 in Supplement 1], which have better coupling to the HMM modes than horizontal dipoles and therefore also experience a larger Purcell enhancement (Section 3 of Supplement 1). Since the vertical dipole moment experiences a larger Purcell enhancement (see Fig. S2 in Supplement 1), the average lifetime within the grating is shorter (see Section 7 of Supplement 1).

Even with optimized grating design, the total number of outcoupled photons is eventually restricted by material loss in metal–dielectric structures such as the one shown here. In this context, the recent work on low-loss HMMs with extremely high PDOS [14] provides an ideal platform to implement such outcoupling mechanisms for embedded emitters. HCGs can be realized with a variety of CMOS-compliant materials. This advantage promises increased efficiency in the near infrared, where the loss in materials such as Ge and Si is lower.

In summary, we present an active HMM with a high-index-contrast grating that provides both enhancement in the SE rate and efficient light extraction of high-k modes into the far field. We show reduction in the SE lifetime by a factor of ∼10 along with a factor of ∼20 enhancement in light extraction from QD emitters embedded inside the HMM. Control of SE and extraction of light from active HMMs is an important step in achieving practical photonic devices such as subwavelength lasers, superluminescent LEDs, and single–photon sources.

FUNDING INFORMATION

Army Research Office (ARO) (W911NF1310001); Army Research Office - MURI; Helmholtz Alberta Initiative; National Science Foundation - MRSEC (1120923); Natural Sciences and Engineering Research Council of Canada (NSERC).

ACKNOWLEDGMENT

The authors thank Mircea Cotlet and Huidong Zang and Yun Yu for assistance with experimental work. Research was carried out in part at the Center for Functional Nanomaterials, Brookhaven National Laboratory, which is supported by the U.S. Department of Energy, Office of Basic Energy Sciences, under Contract No. DE-AC02-98CH10886.

See Supplement 1 for supporting content.

REFERENCES

1. R. Lo Savio, S. L. Portalupi, D. Gerace, A. Shakoor, T. F. Krauss, L. O'Faolain, L. C. Andreani, and M. Galli, Appl. Phys. Lett. **98**, 201106 (2011).
2. S. L. Portalupi, M. Galli, C. Reardon, T. F. Krauss, L. O'Faolain, L. C. Andreani, and D. Gerace, Opt. Express **18**, 16064 (2010).
3. Z. Jacob, I. I. Smolyaninov, and E. E. Narimanov, Appl. Phys. Lett. **100**, 181105 (2012).
4. I. Avrutsky, I. Salakhutdinov, J. Elser, and V. Podolskiy, Phys. Rev. B **75**, 241402 (2007).
5. J. Kim, V. P. Drachev, Z. Jacob, G. V. Naik, A. Boltasseva, and E. E. Narimanov, Opt. Express **20**, 8100 (2012).
6. M. A. Noginov, H. Li, Y. A. Barnakov, D. Dryden, G. Nataraj, G. Zhu, C. E. Bonner, M. Mayy, Z. Jacob, and E. E. Narimanov, Opt. Lett. **35**, 1863 (2010).
7. T. Tumkur, G. Zhu, P. Black, Y. A. Barnakov, C. E. Bonner, and M. A. Noginov, Appl. Phys. Lett. **99**, 151115 (2011).
8. D. Lu, J. J. Kan, E. E. Fullerton, and Z. Liu, Nat. Nanotechnol. **9**, 48 (2014).
9. H. N. S. Krishnamoorthy, Z. Jacob, E. Narimanov, I. Kretzschmar, and V. M. Menon, Science **336**, 205 (2012).
10. K. V. Sreekanth, K. H. Krishna, A. De Luca, and G. Strangi, Sci. Rep. **4**, 6340 (2014).
11. W. D. Newman, C. L. Cortes, and Z. Jacob, J. Opt. Soc. Am. B **30**, 766 (2013).
12. A. S. Potemkin, A. N. Poddubny, P. A. Belov, and Y. S. Kivshar, Phys. Rev. A **86**, 023848 (2012).
13. C. J. Chang-Hasnain and W. Yang, Adv. Opt. Photon. **4**, 379 (2012).
14. G. V. Naik, B. Saha, J. Liu, S. M. Saber, E. A. Stach, J. M. K. Irudayaraj, T. D. Sands, V. M. Shalaev, and A. Boltasseva, Proc. Natl. Acad. Sci. USA **111**, 7546 (2014).